Simple hysteresis loop model for rock magnetic analysis

CARLOS A. VASQUEZ[1,2] AND SABRINA Y. FAZZITO[1]

1 CONICET, Departamento de Geología, IGEBA, Facultad de Ciencias Exactas y Naturales, Universidad de Buenos Aires, Intendente Güiraldes 2160, Pabellón II, Ciudad Universitaria, Ciudad Autónoma de Buenos Aires, Argentina (vasquez@gl.fcen.uba.ar)

2 Universidad de Buenos Aires, Ciclo Básico Común, Ramos Mejía 841, Ciudad Autónoma de Buenos Aires, Argentina

Received: May 31, 2019; Revised: October 21, 2019; Accepted: November 28, 2019

ABSTRACT

A simple phenomenological model founded on Lorentzian functions is evaluated on the first derivative of magnetic hysteresis loops from several artificial samples with iron oxide/oxyhydroxide mixtures imitating natural sediments. The approach, which shows that hysteresis loops can be described by elementary analytical functions and provides estimates of magnetization parameters to a satisfactory degree of confidence, is applied with the help of standard data analysis software. Distorted hysteresis loops (wasp-waisted, goose-necked and pot-bellied shaped) from simulations and artificial samples from a previous work are reproduced by the model which allows to straightforwardly unmix the ferromagnetic signal from different minerals like magnetite, greigite, haematite and goethite. The analyses reveal that the contribution from the ferrimagnetic fraction, though present in a minor concentration (≤ 2.15 wt%), dominates the magnetization.

Keywords: magnetic hysteresis loops, Lorentzian functions, iron oxides/oxyhydroxides, rock magnetism

1. INTRODUCTION

Mathematical modelling of magnetic hysteresis loops has not only gathered a great interest in industrial applications (*Kwun and Burkhardt, 1987*; *Wang et al., 2016*; *Kobayashi et al., 2018*), as well as in rock magnetism and materials science (*Mayergoyz, 1986*; *Hodgdon, 1988*; *Jackson et al., 1990*; *Carter-Stiglitz et al., 2001*, among others). In materials that are exclusively constituted of magnetic grains such as iron, steel, ferrites, magnetic alloys and rare earths, unfortunately, modelling displays several drawbacks as the result of diverse complex phenomena like interactions between neighbouring grains, demagnetizing effects associated with sample shape and, in the case of metals, magnetic permeability.

In palaeomagnetism and environmental magnetism hysteresis loops have been used as a tool to identify magnetic minerals, concentrations, spin ordering, particle size and domain state (e.g., *Stoner and Wohlfarth, 1948*; *Schmidbauer and Schembera, 1987*;

Stud. Geophys. Geod., 64 (2020), 114–129, DOI: 10.1007/s11200-019-1942-8

Dunlop and Özdemir, 1997; *Bertotti, 1998*; *Dunlop 2002a,b*; *Tauxe et al., 2002*; *Fabian, 2003*). Natural sediments, in particular, arouse special interest as these are usually characterized by low concentrations (< 1 wt%) of paramagnetic and ferromagnetic (s.l.) grains dispersed in a non-conductive diamagnetic matrix and hence, in first approximation, the problem simplifies as secondary effects can be neglected. The characterization of distinct coercitivity populations present in a rock from magnetization measurements has been used to elucidate the origin of natural mineral assemblages and to reveal different environmental processes (*Jackson et al., 1993*; *Channell and McCabe, 1994*; *Tauxe et al., 1996*; *Tauxe, 1998*; *Heslop; 2015*), establishing the unmixing of hysteresis loops into individual components as a key concern for rock-magnetism research. Several models have been suggested for decomposing magnetic hysteresis loops, like those which apply approximation by multi-variate functions (*Thompson, 1986*), Fourier analysis (*Willcock and Tanner, 1983*; *Upda and Lord, 1985*; *Josephs et al., 1986*; *Jackson et al., 1990*), second-order rational functions (*Rivas et al., 1981*), hyperbolic basis functions (*von Dobeneck, 1996*); singular value decomposition (*Carter-Stiglitz et al., 2001*), sigmoid logistic functions (*Jackson and Solheid, 2010*) and numerical estimation of end-members (*Heslop and Roberts, 2012*; *Zhang et al., 2016*). However, sometimes these are difficult to implement and the availability of software packages for processing and analysing magnetic hysteresis data is still scarce (*von Dobeneck, 1996*; *Paterson et al., 2018*).

In this paper, hysteresis loops of artificial samples, with concentrations of synthetic/natural iron oxides/oxyhydroxides typical in sediments, are used to test the reliability of a basic phenomenological model grounded on Lorentzian functions with the aim to discriminate magnetic phases, characterize magnetic properties and reproduce the shape of distorted magnetization loops with the assistance of traditional data analysis software. Hysteresis parameters are estimated from direct measurements and then compared to those obtained from the model fitted to the first derivative of the magnetization. Unmixing of magnetization is assessed on simulated distorted hysteresis loops and on wasp-waisted loops from well-characterised mixtures of artificial samples reported in a previous work by *Roberts et al. (1995)*.

2. THEORETICAL MODEL

Jiles and Atherton (1984) and *Jiles and Thoelke (1989)* studied the mathematical shape of the sigmoidal hysteresis loops and found that for major loops the relationship between the magnetization M and the magnetic field can be expressed as:

$$M = L\left(\frac{B_e}{a}\right) - \kappa\delta\left(L'\left(\frac{B_e}{a}\right) - L'\left(\frac{B_{e\,max}}{a}\right)\right) + \kappa^2 L^2\left(\frac{B_e}{a}\right), \tag{1}$$

where L is the Langevin function (function of B_e/a, L' and L'' indicate first and second derivative, respectively), B_e the effective flux density, $B_{e_{max}}$ the maximum B_e experienced by the sample, $a = k_B T/m$ (k_B is the Boltzmann constant, T is the absolute temperature in Kelvin and m is the magnetic moment per unit volume), and κ and δ are

coefficients (*Jiles and Atherton, 1984*). The expression for the magnetization in Eq. (1) can be approximated by the summation of a linear term and an arctan function as follows:

$$M(x) = \int y(x)\,dx = y_0 x + \frac{A}{\pi}\arctan\left(\frac{2(x - x_c)}{w}\right), \tag{2}$$

where x is the independent variable (magnetic field) and y_0, A, w and x_c are function parameters explained later. Equation (2) reproduces the lower branch of the hysteresis loop in the interval $\left[-B_m, B_m\right]$ if $x_c > 0$. B_m represents the maximum applied field. The upper branch that completes the loop is found by changing x_c to $-x_c$ in Eq. (2).

As a consequence, in this work, an elemental phenomenological model based on the Lorentzian function, which is the derivative of M in Eq.(2)

$$y(x) = y_0 + \frac{2A}{\pi}\left[\frac{w}{4(x - x_c)^2 + w^2}\right], \tag{3}$$

where x represents the magnetic field, is proposed to describe the first derivative of the hysteresis loop in view that the primitive integral of Eq. (3) is expressed, as well as the magnetization, in terms of an arctan function. Using this approach, Eq. (3) represents the variation of the magnetic susceptibility with field.

Consequently, simple relationships between the parameters y_0, A, w and x_c of the Lorentzian function from Eq. (3) and typical magnetic hysteresis parameters are established by evaluating the expression for the magnetization (Eq. (2)) as follows ahead.

The high-field (dia- or paramagnetic) susceptibility, χ_p, is given by the slope of the linear term of the magnetization in Eq. (2):

$$\chi_p = y_0 . \tag{4}$$

By definition, the magnitude of the coercive force B_c is determined when the ferromagnetic contribution to the magnetization, i.e. the second term of Eq. (2), is zero, which determines a relationship with the x_c parameter:

$$B_c = x_c . \tag{5}$$

The saturation magnetization M_s is given by the limit of the second (non-linear) term of Eq. (2) when x approaches infinity:

$$M_s = \frac{A}{2} . \tag{6}$$

The saturation remanence M_{rs} is defined as the magnetization at zero field, thus:

$$M_{rs} = M(0) = \frac{A}{\pi}\arctan\left(\frac{-2x_c}{w}\right). \tag{7}$$

The initial magnetic susceptibility χ_i is the derivative of the magnetization (Eq. (2)) at the zero magnetic field, i.e. Eq. (3) evaluated at $x = 0$:

$$\chi_i = \left.\frac{dM}{dH}\right|_{H=0} = y(0) = y_0 + \frac{2A}{\pi}\left(\frac{w}{4x_c^2 + w^2}\right). \tag{8}$$

The ferromagnetic magnetic susceptibility χ_f is obtained by subtracting the paramagnetic susceptibility χ_p from the initial susceptibility χ_i:

$$\chi_f = \chi_i - \chi_p = \frac{2Aw}{\pi\left(4x_c^2 + w^2\right)}. \tag{9}$$

3. MATERIALS AND METHODS

Seventeen samples were prepared in an ARALDITE diamagnetic epoxy resin cement matrix with mixtures of five powdered ferromagnetic (s.l.) substances, in different concentrations (Table 1), including: i) single-domain magnetite (SDM), ii) multi-domain magnetite (MDM), iii) haematite with magnetite and/or maghemite impurities (HE), iv) pure haematite (HET) and v) goethite with magnetite and/or maghemite impurities (GO). SDM, HE and GO are three well-characterized BAYFERROX (Bayer Co.) synthetic iron oxide/oxyhydroxide pigments: 318 BR, 732M BR and 920LO BR, respectively. The BAYFERROX 318 BR pigment was previously described as spherically shaped single-domain magnetite with a mean diameter of ~86 nm (*Vasquez et al., 2018*). HET was obtained by heating the HE powder at 700°C for two hours in an ASC Scientific dual-chamber furnace; the destruction of impurities was confirmed by a one order of magnitude or greater decrease in magnetic susceptibility after thermal treatment. Acquisition of isothermal remanent magnetization (IRM) curves for the HET and HE powdered samples are shown in the Appendix A. In the case of the GO powder, thermal demagnetization cannot be used to eliminate the magnetite/maghemite magnetic moments because the goethite contribution itself would be demagnetized at its Curie temperature ($T_C \approx 130$°C). MDM is a natural magnetite sample. A total concentration of ferromagnetic (s.l.) powder usually of about 2 wt% per sample was pursued to simulate natural conditions. Powder and resin were weighted on an analytical balance with 0.1 mg of accuracy and mixed at least 15 minutes. *Vasquez et al. (2018)* showed that the epoxy resin prevents magnetic interactions and that the BAYFERROX (Bayer Co.) magnetite powder presents a strong SD behaviour. These samples cover the basic spectrum of iron oxide/oxyhydroxide combinations found in natural sediments.

Magnetic hysteresis loops were acquired for each of the samples (Table 1) from –1.5 to 1.5 T, at room temperature, by means of a MicroMag 2900 alternating-gradient magnetometer (Princeton Measurement Corp.) with a sampling rate of 1124 points per loop.

The simplicity that follows from modelling the derivatives of the hysteresis loops by Lorentzian functions allows to resolve the unmixing problem by any standard data

Table 1. Artificial samples prepared with mixtures of natural or synthetic iron oxides/oxyhydroxides in diamagnetic cement matrix. Concentrations of different substances are indicated. The total ferromagnetic (*sensu lato*) abundance per sample is usually around 2 wt%. SDM: single-domain magnetite; MDM: multi-domain magnetite; HE: haematite with magnetite and/or maghemite impurities, HET: pure haematite; GO: goethite with magnetite and/or maghemite impurities.

Sample Code	SDM	MDM	HE	HET	GO	Total
GO1	0.00	0.00	0.00	0.00	2.22	2.22
HEX	0.00	0.00	5.21	0.00	0.00	5.21
HG25	0.00	0.00	0.00	0.57	1.64	2.21
HG50	0.00	0.00	0.00	1.10	1.10	2.20
HG75	0.00	0.00	0.00	1.66	0.55	2.21
SDVII	2.15	0.00	0.00	0.00	0.00	2.15
MD1	0.00	2.12	0.00	0.00	0.00	2.12
HGS33	0.74	0.00	0.00	0.73	0.73	2.20
SHG66	1.32	0.00	0.00	0.34	0.34	2.00
GS25	1.62	0.00	0.00	0.00	0.57	2.19
GS75	0.60	0.00	0.00	0.00	1.61	2.21
HS25	1.61	0.00	0.00	0.59	0.00	2.20
HS50	1.10	0.00	0.00	1.11	0.00	2.21
MH33	0.00	0.84	0.00	1.73	0.00	2.57
MG33	0.00	1.19	0.00	0.00	2.12	3.31
MGH33	0.00	1.48	0.00	1.04	1.03	3.55
HMS33	0.64	1.29	0.00	0.70	0.00	2.63

analysis computer program such as the proprietary software Origin (OriginLab Corp.) or the free available software QtiPlot, SciDAVis, and LabPlot.

The unmixing method was applied at the beginning to experimental data from samples SDVII, HEX and GO1 (SDM, HE and GO powders in epoxy resin matrix, respectively; Table 1) as a first attempt to evaluate the phenomenological model. Initially, the background noise of the upper branches of the hysteresis loops was reduced using the Savitzky-Golay method (second order polynomial). For each of the samples, a Lorentzian function (Eq. (3)) was adjusted to the first derivative of the smoothed upper branch of the hysteresis loop (not slope corrected). In cases with more than one distinct coercivity population, multiple peaks may be observed and the modelling requires to add as many Lorentzian functions as peaks are resolved by visual inspection of the derivative of the (smoothed) measured hysteresis loop. A Levenberg-Marquardt iteration algorithm was used for the Lorentzian non-linear curve fit until the Chi-square tolerance value of 10^{-9} was reached. The y_0, A, w and x_c fitting parameters were used to determine the associated arctangent functions (Eq. (2)) which were compared to the measured magnetic hysteresis loop. To avoid biasing the results, the hysteresis loop was analysed without para- or diamagnetism correction.

The model was subsequently examined in 15 selected samples from Table 1 by contrasting the hysteresis parameters that were obtained from direct measurements to those estimated from Eq. (5) to Eq. (8) after fitting the Lorentzian functions (Eq. (3)) to

the derivatives of the smoothed upper branch of the magnetic hysteresis loops (not slope corrected).

The hysteresis parameters χ_i, M_s, M_{rs}, and B_c of these samples were estimated according to different procedures, after the diamagnetic contribution from the resin cement matrix was removed by subtraction of the high-field slope (χ_{hf}), as follows: i) χ_i: mean value between the two slopes obtained from the linear regressions fitted to the upper and the lower hysteresis branches from –0.05 to 0.05 T; ii) M_s: mean value of the last ten consecutive magnetization measurements (absolute values) at positive and negative high-field extremes; iii) M_{rs}: mean value between the two intercepts given by the linear regressions calculated in (i); iv) B_c: the mean value between the two ratios intercept/slope of the linear fits adjusted in (i). The high-field slope used to remove the diamagnetic background was estimated at each sample by averaging the two slopes obtained from the linear regressions fitted to the last thirty consecutive magnetization measurements at positive and negative high-field extremes. This method assures that for field values above ~1 T the magnetization curve is considered linear. The coefficients of determination of the regression lines are above 0.80 for all calculations, but in most of the cases these are higher than 0.90.

The phenomenological model was also used to unmix five distorted hysteresis loops: three simulated loops (wasp-waisted, goose-necked and pot-bellied shaped, as defined by, e.g., *Tauxe et al., 1996* and *Tauxe, 1998*) and two wasp-waisted loops from artificial samples obtained from data published by *Roberts et al. (1995)*.

4. RESULTS AND DISCUSSION

4.1. Tests on artificial samples with iron oxide/oxyhydroxide mixtures

The magnetic hysteresis loops (upper branches) on artificial samples with synthetic/natural iron oxide/oxyhydroxide mixtures (Table 1) before high-field correction are shown in Fig. 1. The magnetization of samples containing goethite (GO), impure haematite (HE) and mixtures of pure haematite (HET) with goethite (GO) is dominated by diamagnetism with a subordinate ferromagnetic contribution (samples GO1, HEX, HG25, HG50 and HG75; Fig. 1a). In samples with mixtures comprising SDM and/or MDM powder in addition to goethite and/or pure haematite pigments (HGS33, SHG66, GS25, GS75, HS25 MH33, MG33, MGH33 and HMS33; Fig. 1b,c), in the sample SDVII containing only single-domain magnetite (Fig. 1b), or in the sample MD1 involving only natural multi-domain magnetite (Fig. 1c) the magnetization presents a minor to negligible influence from the diamagnetic matrix and it is controlled, instead, by ferromagnetism.

The results of the phenomenological model tested on samples SDVII, HEX and GO1 are initially analysed as examples. The first derivative of the smoothed magnetization (upper branch of the hysteresis loop) and the fitted Lorentzian functions with the associated parameters are shown in Fig. 2a,c,e for each sample, while the hysteresis loops (upper and lower branch) obtained from the magnetization measurements and from the mathematical model (as a composition of two arctangents) are displayed together for comparison in Fig. 2b,d,f. The lower branches are directly obtained by changing x_c to $-x_c$

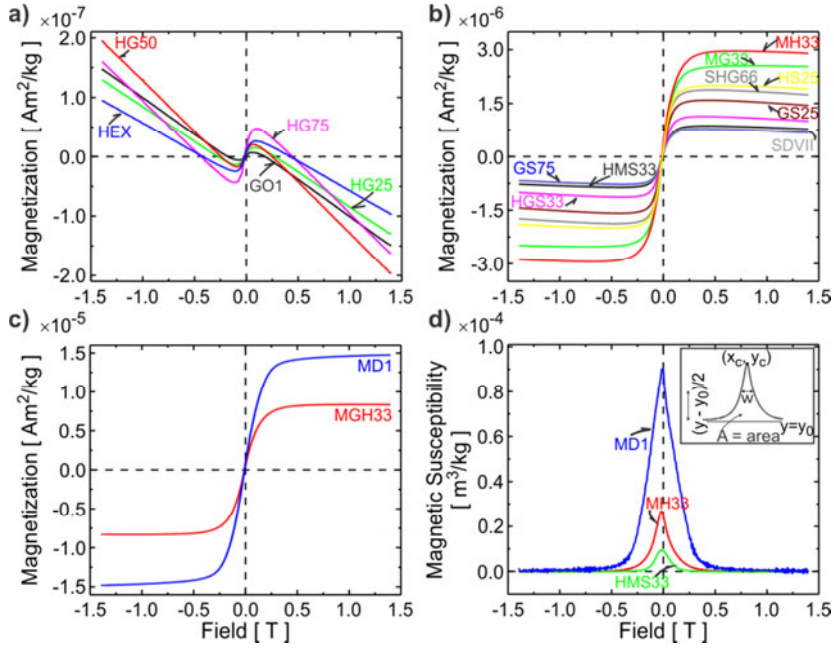

Fig. 1. Hysteresis loops of artificial samples from Table 1 (upper branches): **a)** samples with magnetization dominated by diamagnetism from the matrix; **b)** samples controlled by ferromagnetism with a subordinate diamagnetic contribution; **c)** samples governed by ferromagnetism with a negligible diamagnetic contribution; **d)** dependence of magnetic susceptibility with field for three representative samples determined from differentiation of measured hysteresis loops (upper branches). Inset: parameters of the Lorentzian function.

in Eq. (2).Though in sample SDVII some discrepancy between the measured and the modelled loop is observed predominantly for the high-field negative slope, in general the magnetization data are reproduced reasonably well by the model.

The magnetic parameters χ_i, M_s, M_{rs} and B_c of most of the samples from Table 1, which were estimated from direct measurements and from fitting Lorentzian functions to the derivative of the smoothed hysteresis loops (upper branch), were compared by cross-plots (modelled against measured magnetic parameters; Fig. 3). A least squares linear regression was fitted then to each data set. The coefficients of determination indicate a very good fit with values ranging from 0.99557 to 0.99961, which support the reliability of the Lorentzian model. The plot associated to the B_c magnetic parameter shows the most dispersed points and the lowest coefficient of determination. The slope values 1.0138, 1.307, 1.2853 and 1.2292 for χ_i, M_s, M_{rs} and B_c, respectively, indicate a departure from the expected value of 1 and shows that the best accordance is observed for χ_i (Fig. 3a). Though higher discrepancies are found for M_s, M_{rs} and B_c (Fig. 3b,c,d), the magnetic parameters inferred from the phenomenological model reproduce the trend of those obtained from the hysteresis measurements. The slope values can be used as correction

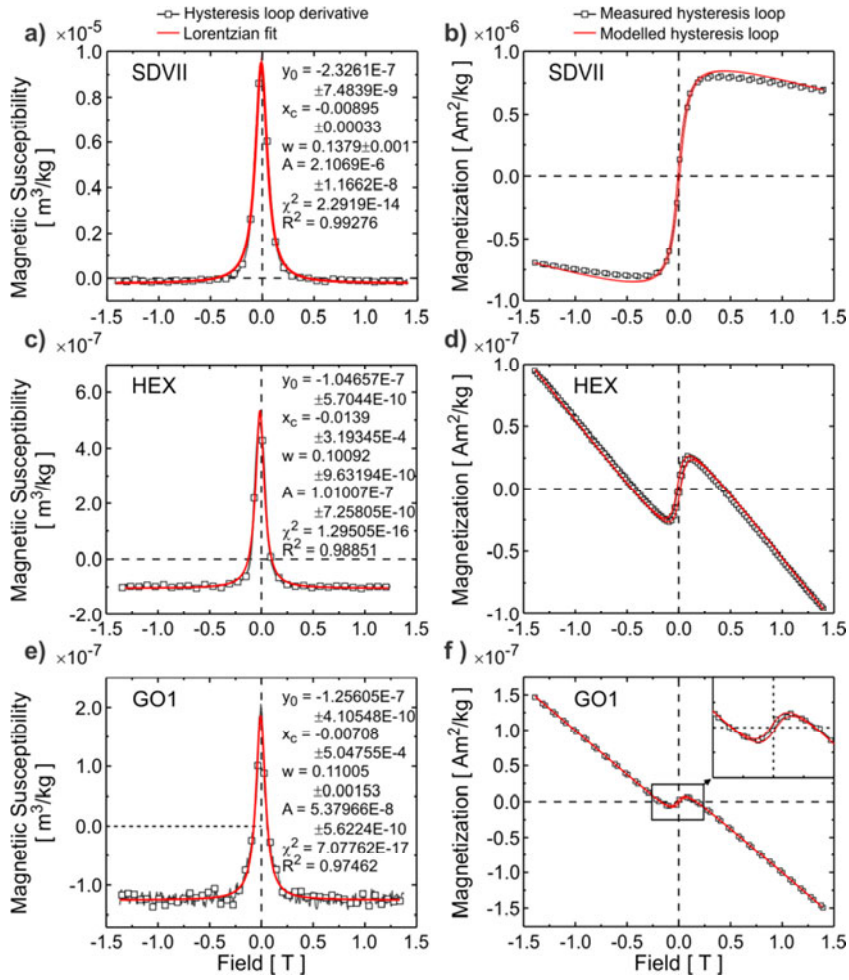

Fig. 2. **a)**, **c)**, **e)** Magnetic susceptibility variation with magnetic field of samples SDVII, HEX and GO1, respectively, obtained from differentiation of the smoothed measured hysteresis loops (upper branches), along with the Lorentzian fitted model curve and the corresponding parameters (see Eqs (3)-(6) for their meaning). **b)**, **d)**, **f)** Comparison between measured and modelled magnetic hysteresis loops of samples SDVII, HEX and GO1, respectively. Smoothed curves are not shown. The negative slopes at high field are due to the diamagnetic contribution from the matrix.

factors to better estimate each magnetic parameter. The noise amplification due to differentiation of smoothed hysteresis loops is possibly a source of these differences. Non-saturation of samples containing goethite and haematite (field values are below 1.5 T; see Appendix A for haematite IRM curves) may be contributing to the misfit of the model as well. In fact, the saturation magnetization M_s is the magnetic parameter which presents the

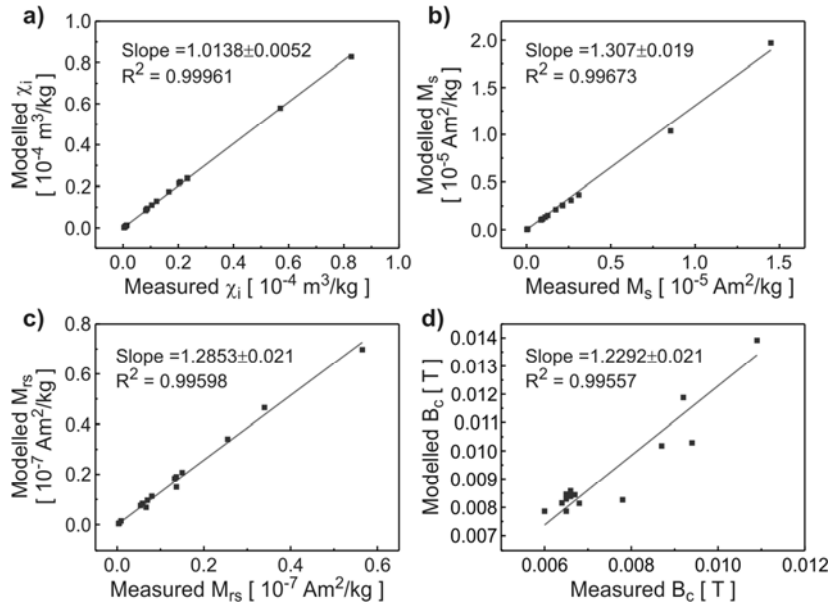

Fig. 3. Comparison between hysteresis parameters from direct measurements and from the model. χ_i: initial magnetic susceptibility, M_s: saturation magnetization, M_{rs}: saturation remanent magnetization, B_c: coercive force. Data were fitted using linear regression forced to zero. The slope and the coefficient of determination R^2 are shown.

higher misfit, with a relative error around 30%. The typical low B_c values (Fig. 3d) observed for all the samples are compatible with the existence of magnetite. Some samples that contain mixtures of haematite and goethite (HG25, HG50 and HG75) have B_c values higher than most of the samples (Fig. 3d). However, an effect due to haematite is not suggested since distorted hysteresis loops typical of mixtures with contrasting coercivities (wasp-waisted, goose-necked or pot-bellied shaped) were not observed. This feature is probably due to magnetite impurities in the goethite powder (GO) that were not possible to be removed by thermal heating. These results indicate that, when magnetite is present, even in low concentrations, the influence of the antiferromagnetic fraction is negligible. Considering that the proportions of magnetic substances in these samples intend to reproduce natural conditions, this study suggests that though haematite and goethite are abundant in sediments, ferrimagnetic minerals, with concentrations below 2.15 wt% (Table 1), control the magnetic behaviour, which is in accordance with the previous findings of *Lagroix and Guyodo (2017)* who found that the magnetic properties in a mixture of magnetite, haematite and goethite are governed by magnetite with a concentration of only 2.3 wt%.

4.2. Tests on simulated distorted wasp-waisted, goose-necked and pot-bellied loops

Distorted hysteresis loops (*Tauxe et al., 1996*; *Tauxe, 1998*) are observed in natural samples when mixtures of ferromagnetic (s.l.) substances show comparable magnetizations and strongly contrasting coercivities (different phases and/or domain state).

In the artificial samples of this work, though mixtures of ferromagnetic (s.l.) substances with very different coercivities are present, the magnetization from haematite and goethite is two or three orders of magnitude below the magnetic signal from magnetite, leading to hysteresis loops without distortions. Consequently, three types of loops, wasp-waisted, goose-necked and pot-bellied shaped (Fig. 4a,c,e, respectively), were simulated. For each loop, two arctangent functions (Eq. (2)) were added representing two magnetic phases with contrasting coercivities and different magnetization intensities. The mathematical model was fitted to the derivative of the lower branches of the total magnetization (Fig. 4b,d,f) by means of a composition of two Lorentzian functions and so the parameters y_0, x_c, w and A of each magnetic phase were obtained for the mixtures. The susceptibility curves exhibit two peaks which are related to different coercivities. In the case of the wasp-waisted and the goose-necked loops, the higher magnetic susceptibility peak is associated to the lower coercivity component, while the lower peak is related to the higher coercivity component. The opposite situation occurs for the pot-bellied loop: the lower susceptibility peak corresponds to the lower coercivity component while the highest susceptibility peak is connected to the higher coercivity component. The magnitudes of the magnetic parameters regulate the distortion of the loops. The w parameter determines the full width at half maximum of the Lorentzian function, which is related to M_{rs} and B_c (Eq. (7)). The mathematical model shows then that the wasp-waisted, the goose-necked and the pot-bellied loops originate from mixtures with high contrasting coercitivity values (discrepancy of one order of magnitude).

4.3. Test on artificial samples with iron oxide/oxyhydroxide/iron sulphide mixtures: wasp-waisted hysteresis loops

Finally, the unmixing method of modelling Lorentzian functions to the derivative of magnetic hysteresis loops was accomplished on data from mixtures of PSD magnetite plus haematite and SD greigite plus haematite reported by *Roberts et al. (1995)*. Data tables of hysteresis loops were reconstructed from the published graphs (Fig. 4a,b from *Roberts et al., 1995*) and a locally weighted scatterplot smoothing (LOWESS) with a proportion 0.1 for span was subsequently applied (Fig. 5a,c). The derivatives of the upper and lower branch for each hysteresis loop were calculated. Two clear main peaks were identified for each derivative and a Lorentzian fit (Fig. 5b,d) was carried out by a multi-peak procedure (see, e.g., OriginLab, QtiPlot and SciDAVis), though a typical non-linear curve fit by summation of two Lorentzian functions can be chosen. The fitting parameters y_0, A, w and x_c were estimated for each peak (Fig. 5b,d) and then used to obtain the expression for the magnetization (Eq. (2)) as a sum of two arctangents (Fig. 5a,c).

The best results were obtained from the model applied to the derivative of the lower branch of the smoothed PSD magnetite plus haematite curve and to the upper branch of the smoothed SD greigite plus haematite curve, so we only reproduce the data and the curves from these cases (Fig. 5, Table 2). The magnetic parameters B_c, M_s and M_{rs} of the pure samples from *Roberts et al. (1995)* are compared in Table 2 with those estimated from Eqs (5)–(7), fitted for each sample. The corresponding relative errors (Table 2) were determined as ratios of the modelled to the measured (*Roberts et al., 1995*) values. It is observed that, except for one case, all the relative errors are below 29%. The model

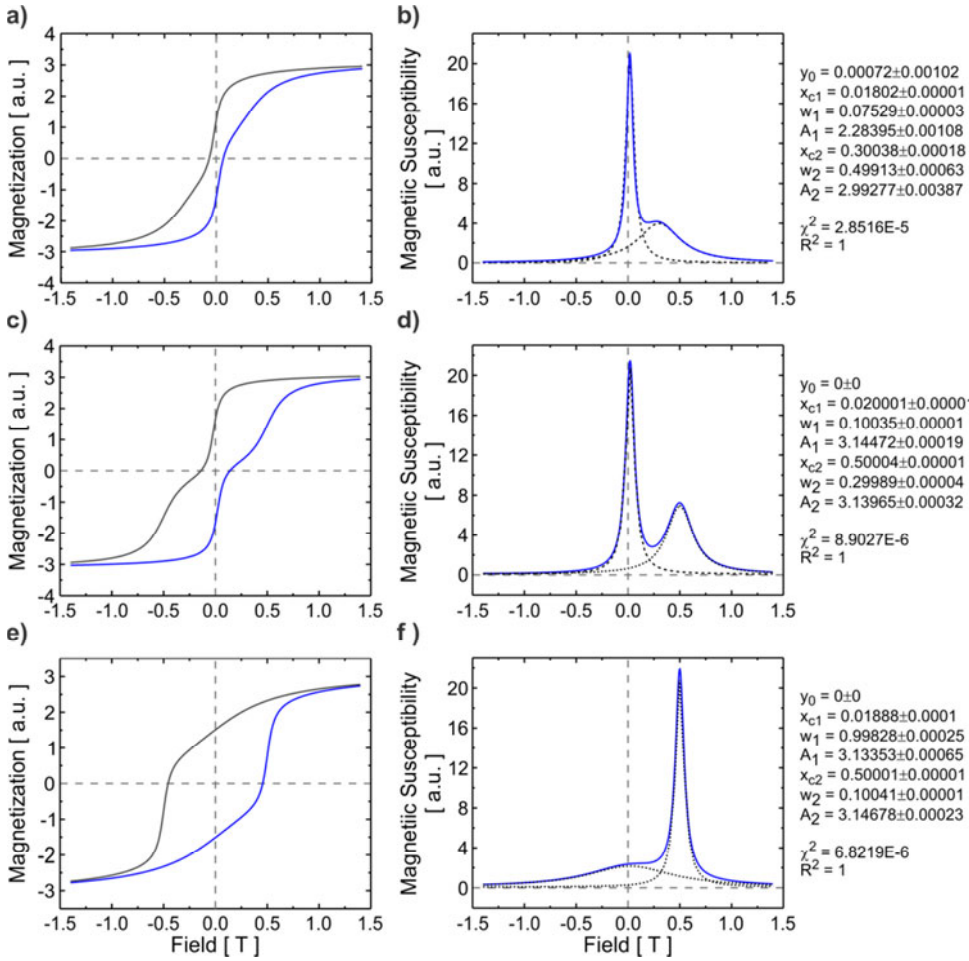

Fig. 4. Simulated **a)** wasp-waisted, **c)** goose-necked and **e)** pot-bellied magnetic hysteresis loops from mixtures of two magnetic components with contrasting coercitivities; **b)**, **d)** and **f)** 2-component model of the corresponding lower-branch first derivatives (magnetic susceptibility), respectively, along with the parameters of the Lorentzian fit, see Eqs (3)–(6) for their meaning.

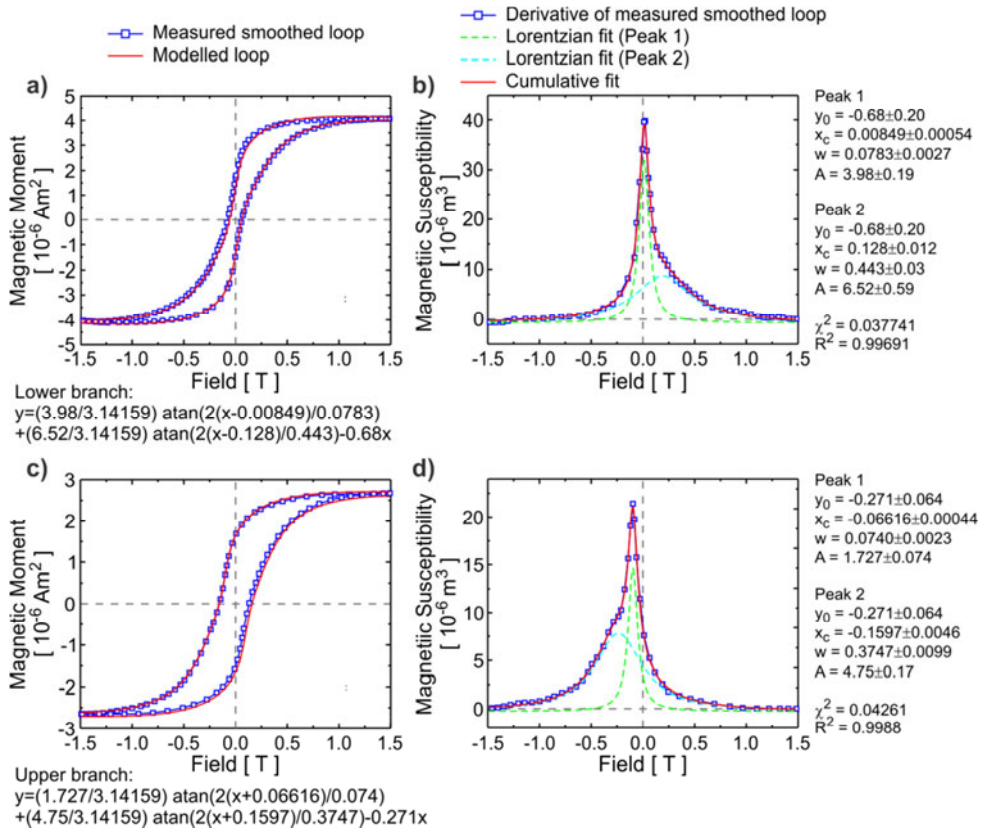

Fig. 5. Lorentzian model tested on two distorted (wasp-waisted) magnetic hysteresis loops from reconstructed data of artificial mixtures published by *Roberts et al. (1995)*. **a)** Comparison between measured and modelled magnetic hysteresis loops for pseudo-single-domain (PSD) magnetite plus haematite; **b)** susceptibility as a function of the magnetic field for the PSD magnetite plus haematite, as obtained from differentiation of the lower branch of the smoothed measured hysteresis loop (*Roberts et al., 1995*); **c)** and **d)** the same as in a) and b), respectively, but for the single-domain (SD) greigite plus haematite, and susceptibility in d) obtained from differentiation of the upper branch of the smoothed measured hysteresis loop (*Roberts et al., 1995*). The Lorentzian fitted model with the associated parameters for each peak and the cumulative fit are shown.

determines an extraordinary high value of 60% for the misfit of the M_S in the PSD magnetite + haematite sample, which can be due to an effect of the non-saturation of haematite, as these hysteresis loops were obtained with fields below 1 T. Though the modelling of derivatives by a Lorentzian fit does not always provide estimates of magnetization parameters to a high degree of confidence, it is a straightforward approximation to unmix magnetic phases from magnetic hysteresis curves and a new alternative for identification of ferromagnetic mineralogy.

Table 2. Results of unmixing the distorted magnetic hysteresis loops. Comparison of experimentally determined magnetic parameters for pure samples (*Roberts et al., 1995*) with those estimated from Lorentzian functions fitted by the derivative of the smoothed hysteresis loops of mixtures of pseudo-single-domain (PSD) magnetite + haematite and single-domain (SD) greigite + heamatite. B_c: coercive force, M_S: saturation magnetization, M_{rs}: saturation remanent magnetization, *Er*: corresponding relative error.

Sample	Component or Peak	Reference	B_c [T]	$Er(B_c)$	M_s [10^{-6} Am^2 kg^{-1}]	$Er(M_s)$	M_{rs} [10^{-6} Am^2 kg^{-1}]	$Er(M_{rs})$
PSD Magnetite + Haematite	1 (magnetite)	Measured*	0.0087	0.97	1.80	1.10	0.29	0.93
		Model (this study)	0.0085		1.99		0.27	
	2 (haematite)	Measured*	0.1500	0.86	1.98	1.60	1.19	0.91
		Model (this study)	0.1280		3.26		1.09	
SD Magnetite + Haematite	1 (greigite)	Measured*	0.0538	1.23	0.81	1.07	0.45	1.29
		Model (this study)	0.0662		0.86		0.58	
	2 (haematite)	Measured*	0.1500	1.06	1.98	1.19	1.19	0.89
		Model (this study)	0.1597		2.38		1.07	

* *Roberts et al. (1995)*

5. CONCLUSIONS

The first derivative of magnetic hysteresis loops from several artificial samples comprising mixtures of ferromagnetic minerals, in concentrations typically found in natural sediments, was modelled using Lorentzian functions allowing to associate magnetic properties of ferromagnetic (s.l.) substances with fitting parameters. Though magnetic parameters cannot be estimated by this approach to a high level of confidence, the shape of distorted hysteresis loops, which is originated from mixtures of substances with contrasting coercivities, were very well reproduced allowing to unmix the different magnetic phases of simulated loops and artificial samples.

This simple Lorentzian model avoids complex baseline and high-field corrections and it is particularly useful when dealing with distorted hysteresis loops; in other cases, however, the classical direct methods to estimate hysteresis parameters is still recommended. The use of analytical functions allows to assess the resolution of the

magnetic hysteresis loop decomposition problem by means of a rapid and practical method which is possibly to apply by means of any easy available software that includes simple non-linear fitting procedures instead of specific unmixing software.

The study also exhibits that the characteristics of the magnetic signal of natural sediments is dominated by the properties of the ferrimagnetic fraction, though present in minor concentrations (≤ 2.15 wt%).

APPENDIX A

Acquisition of isothermal remanent magnetization curves for the BAYFERROX 732M BR powdered pigment before (Fig. A.1a, HE) and after (Fig. A.1b, HET) thermal treatment showing different magnetic behaviour. For the HE sample saturation occurs at ~1.5 T due to the presence of magnetite and/or maghemite impurities while for the HET sample saturation is not reached even at the maximum applied field of 9 T. The coercivity of remanence is indicated for each sample.

Acknowledgements: We are very grateful to Liliana Castro (Dpto. Cs. Geológicas, FCEN, UBA) for generously supplying the MDM powder. The analytical balance was kindly provided by Dpto. de Química Inorgánica, Analítica y Química Física (FCEN, UBA). Hysteresis loops of artificial samples were measured at Instituto de Geofísica (Universidad Nacional Autónoma de México). This research benefited from Agencia Nacional de Promoción Científica y Tecnológica (Grant 014-1516). Technical specifications of synthetic powdered samples are available at *http://bayferrox.com*. We are deeply thankful for the insightful comments of two anonymous reviewers and Associate Editor Dr. Mark J. Dekkers which helped to significantly improve the manuscript.

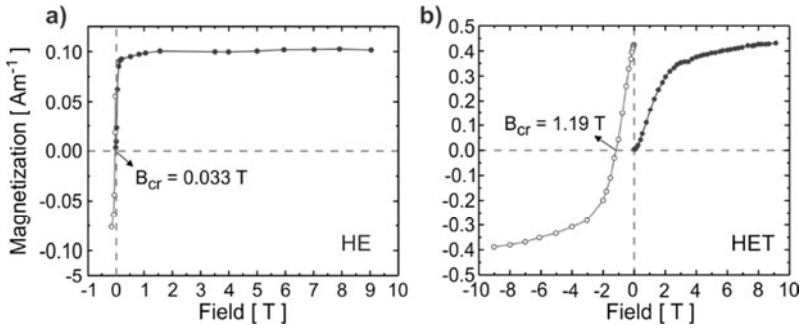

Fig. A1. Acquisition of isothermal remanent magnetization curves for the BAYFERROX 732M BR powdered pigment **a)** before (HE), and **b)** after (HET) thermal treatment, showing different magnetic behaviour. For the HE sample, saturation occurs at ~1.5 T due to the presence of magnetite and/or maghemite impurities while for the HET sample saturation is not reached even at the maximum applied field of 9 T. The coercivity of remanence B_{cr} is indicated for each sample.

References

Bertotti G., 1998. *Hysteresis in Magnetism: For Physicists, Materials Scientists, and Engineers*. First Edition. Academic Press, San Diego, CA.

Carter-Stiglitz B., Moskowitz B. and Jackson M., 2001. Unmixing magnetic assemblages and the magnetic behavior of bimodal mixtures. *J. Geophys. Res.-Solid Earth.*, **106**, 26397–26411.

Channell J.E.T. and McCabe C., 1994. Comparison of magnetic hysteresis parameters of unremagnetized and remagnetized limestones. *J. Geophys. Res.-Solid Earth*, **99**, 4613–4623.

Dunlop D.J. and Özdemir Ö., 1997. *Rock Magnetism: Fundamentals and Frontiers*. Cambridge University Press, Cambridge, U.K.

Dunlop D., 2002a. Theory and application of the Day plot (Mrs/Ms versus Hcr/Hc). 1. Theoretical curves and tests using titanomagnetite data. *J. Geophys. Res.-Solid Earth*, **107(B3)**, 2056.

Dunlop D., 2002b. Theory and application of the Day plot (Mrs/Ms versus Hcr/Hc). 2. Application to data for rocks, sediments and soils. *J. Geophys. Res.-Solid Earth*, **107(B3)**, 2057.

Fabian K., 2003. Some addtional parameters to estimate domain state from isothermal magnetization measurements. *Earth Planet. Sci. Lett*., **213**, 337–345.

Heslop D., 2015. Numerical strategies for magnetic mineral unmixing. *Earth Sci. Rev*., **150**, 256–284.

Heslop D. and Roberts A.P., 2012. A method for unmixing magnetic hysteresis loops. *J. Geophys. Res.-Solid Earth*, **117**, B03103.

Hodgdon M.L., 1988. Mathematical theory and calculations of magnetic hysteresis curves. *IEEE Trans. Magn*., **24**, 3120–3122.

Jackson M., Worm H.-U. and Banerjee S.K., 1990. Fourier analysis of digital hysteresis data: rock magnetic applications. *Phys. Earth. Planet. Inter.*, **65**, 78–87.

Jackson M., Rochette P., Fillion G., Banerjee S. and Marvin J., 1993. Rock magnetism of remagnetized Paleozoic carbonates: low-temperature behavior and susceptibility characteristics. *J. Geophys. Res.-Solid Earth*, **98**, 6217–6225.

Jackson M. and Solheid P., 2010. On the quantitative analysis and evaluation of magnetic hysteresis data. *Geochem. Geophys. Geosyst.*, **11**, Q04Z15,

Jiles D.C. and Atherton D.L., 1984. Theory of ferromagnetic hysteresis. *J. Appl. Phys*., **55**, 2115–2120.

Jiles D.C. and Thoelke J.B., 1989. Theory of ferromagnetic hysteresis: determination of model parameters from experimental hysteresis loops. *IEEE Trans. Magn.*, **25**, 3928–3930.

Josephs R.M, Crompton D.S. and Krafft C.S., 1986. Characterization of magnetic oxide recording media using Fourier analysis of static hysteresis loops. *IEEE Trans. Mag.*, **22**, 653–655.

Kobayashi S., Miura K., Narita Y. and Takahashi S., 2018. Magnetic investigations of steel degradation using a magnetic hysteresis scaling technique. *Metals*, **8**, 1–12.

Kwun H. and Burkhardt G.L., 1987. Effects of grain size, hardness, and stress on the magnetic hysteresis loops of ferromagnetic steels. *J. Appl. Phys*., **61**, 1576–1579.

Lagroix F. and Guyodo Y., 2017. A new tool for separating the magnetic mineralogy of complex mineral assemblages from low temperature magnetic behavior. *Front. Earth Sci*., **5**, 61.

Mayergoyz I.D., 1986. Mathematical models of hysteresis. *IEEE Trans. Magn*., **22**, 603–608.

Paterson G.A., Zhao X., Jackson M. and Heslop D., 2018. Measuring, processing and analyzing hysteresis data. *Geochem. Geophys. Geosyst*., **19**, 1925–1945.

Rivas J., Zamarro J.M., Martín E. and Pereira C., 1981. Simple approximation for magnetization curves and hysteresis loops. *IEEE Trans. Magn*., **17**, 1498–1502.

Roberts A.P., Cui Y. and Verosub K.L., 1995. Wasp-waisted hysteresis loops: Mineral magnetic characteristics and discrimination of components in mixed magnetic systems. *J. Geophys. Res.-Solid Earth*, **100**, 909–924.

Tauxe L., 1998. *Paleomagnetic Principles and Practice*. Modern Approaches in Geophysics **18**. Kluwer Academic Publishers, Dordrecht, The Netherlands.

Tauxe L., Mullender T.A.T. and Pick T., 1996. Potbellies, wasp-waists, and superparamagnetism in magnetic hysteresis. *J. Geophys. Res.-Solid Earth*, **101**, 571–583.

Tauxe L., Bertram H.N and Seberino C., 2002. Physical interpretation of hysteresis loops: Micromagnetic modeling of fine particle magnetite. *Geochem. Geophys. Geosyst*., **3**, 1055, DOI: 10.1029/2001GC000241.

Thompson R., 1986. Modelling magnetization data using SIMPLEX. *Phys. Earth Planet. Inter*., **42**, 113–127.

Schmidbauer E. and Schembera N., 1987. Magnetic hysteresis properties and anhysteretic remanent magnetization of spherical Fe3O4 particles in the grain size range 60-160 nm. *Phys. Earth Planet. Inter.*, **46**, 77–83.

Stoner E.C. and Wohlfarth E.P., 1948. A mechanism of magnetic hysteresis in heterogeneous alloys. *Phil. Trans. R. Soc. London A*, **240**, 599–642.

Upda S.S. and Lord, W., 1985. A Fourier descriptor model of hysteresis loop phenomena. *IEEE Trans. Mag.*, **21**, 2370–2373.

Vasquez C.A., Sapienza F.F., Somacal A. and Fazzito S.Y., 2018. Anhysteretic remanent magnetization: model of grain size distribution of spherical magnetite grains. *Stud. Geophys. Geod.*, **62**, 339–351.

von Dobeneck T., 1996. A systematic analysis of natural magnetic mineral assemblages based on modelling hysteresis loops with coercivity-related hyperbolic basis functions. *Geophys. J. Int.*, **124**, 675–694.

Wang H., Zhan J., Yu Z., Zhang Y., Yu J., Gui Y., Yu T., Xie J., Zhang H., Ji Y., Zan N., Fu R. and Perin D., 2016. A novel hysteresis model of magnetic field strength determined by magnetic induction intensity for Fe-3% Si electrical steel applied in cigarette making machines. *J. Mater.*, ID 1509498, DOI: 10.1155/2016/1509498.

Willcock S.N.M. and Tanner B.K., 1983. Harmonic analysis of B-H loop. *IEEE Trans. Mag.*, **19**, 2265–2270.

Zhang R., Necula C., Heslop D. and Nie J., 2016. Unmixing hysteresis loops of the late Miocene-early Pleistocene loess-red clay sequence. *Sci. Rep.*, **6**, 29515.